JOURNAL OF MATERIALS SCIENCE 30 (1995) 5295–5303

High-temperature flow behaviour and concurrent microstructural evolution in an Al–24 wt% Cu alloy

P. K. BAKSHI*, B. P. KASHYAP
Department of Metallurgical Engineering and Materials Science, Indian Institute of Technology, Bombay 400076, India

Tensile specimens of an Al–24 wt% Cu alloy of grain sizes in the range 7.6–20.6 μm were deformed at 400–540 °C using constant initial strain rates ranging from 5×10^{-6} to 2×10^{-2} s^{-1}. Initially the stress–strain (σ–ε) curves show work hardening which is followed by strain softening at higher strain rates and lower temperatures. At lower strain rates and higher temperatures, on the other hand, σ continues to increase with strain or tends to be independent of strain. Grain growth and cavitation occur to varying extents depending on strain rate and test temperature. While the grain growth can account for the work hardening at higher temperatures as well as at lower strain rates, it fails to do so at higher strain rates. The strain softening is associated with cavitation. The presence of non-steady-state flow influences the parameters of the constitutive relation to varying extents.

1. Introduction

High-temperature deformation behaviour of several materials can be generalized by an empirical relation [1]

$$\dot{\varepsilon} = \frac{AD_0Eb}{kT}\left(\frac{b}{d}\right)^p\left(\frac{\sigma}{E}\right)^n \exp\left(-\frac{Q}{RT}\right) \quad (1)$$

where $\dot{\varepsilon}$ is a strain rate corresponding to the flow stress, σ, grain size, d, and test temperature, T (K), $D_0 \exp(-Q/RT)$ is the appropriate diffusion coefficient with Q being the activation energy, E the Young's modulus, b is the Burger's vector, P is the grain-size exponent, n is the stress exponent, which is equal to the inverse of the strain-rate sensitivity index ($n = 1/m$), A is a dimensionless constant and k, R have their usual meanings. Several theories [2, 3] have been developed to understand the mechanisms of deformation, and to account for the observed magnitudes of p, n, Q, and A in Equation 1.

Two-phase and quasi-single-phase materials, processed to fine equiaxed grains ($d \leqslant 10$ μm), exhibit [4] sigmoidal $\log\sigma$ versus $\log\dot{\varepsilon}$ curves with three sets of m, p and Q values. At low strain rates (Region I), $m < 0.3$, $p = 2$–3, $Q = Q_l$, the activation energy for lattice diffusion; at intermediate strain rates (Region II), $m \approx 0.5$, $p = 2$–3, $Q = Q_{gb}$, the activation energy for grain-boundary diffusion; and at high strain rates (Region III), $m < 0.3$, $p = 0$ and $Q = Q_l$ have been almost established.

The micrograined materials can be deformed to exceptionally large strains without premature failure in Region II. Such superplastic property has been extensively studied [2, 4–6]. While using Equation 1 for characterizing the flow behaviour of superplastic materials, the grain size is considered to be stable and the flow stress is taken to be independent of strain, as believed in the beginning. However, now it is confirmed that several materials exhibit concurrent grain growth [7] and cavitation [8] during superplastic deformation. One such example of superplastic materials is the Al–Cu eutectic alloy [9, 10]. The grain growth and cavitation may lead to a deviation from the steady state whereupon the stress becomes sensitive to strain level; and the values of n, p, Q and A can vary significantly. Although this is realized now, there does not appear to be a systematic study involving grain growth and cavitation behaviour for demonstrating the extent of variations in the parameters of the constitutive relation. Therefore, the aim of the present work was to examine the following three aspects: (i) the nature of the variation in the flow stress as a function of strain at different test conditions, (ii) variation in the apparent values of the parameters of the constitutive relation, and (iii) microstructural evolution and its relation to non-steady state nature of flow. For this purpose, an Al–24 wt % Cu alloy containing the soft aluminium-rich (χ) and the hard $CuAl_2$ (θ) phase in the ratio 60:40 was used.

2. Experimental procedure

The experimental methods employed for the material preparation, tensile test and metallography are described elsewhere [11, 12]. The chemical composition

Present address: Metallurgy Department, Government Engineering College, Raipur 492 010, India

0022–2461

(wt %) of the alloy was analysed to be: 24.38 Cu, 0.29 Fe, 0.05 Si, 0.023 Zn, 0.006 Mn, 0.003 Mg, < 0.005 Pb, < 0.002 Ni, the balance being aluminium. Hereafter, this alloy will be termed Al–24Cu.

Tensile specimens of gauge dimensions 25 mm long, 6 mm wide and 1.8 mm thick, were machined. These specimens were annealed at 535 °C for 24–450 h for producing various grain sizes.

The grain sizes were measured by the mean linear intercept method with no distinction being made between the χ and θ phases. The grain sizes reported here have an accuracy of $\pm$ 10% at the 95% confidence level.

In order to determine the cavity volume, the densities of both the gauge and shoulder sections of the deformed specimens were determined by weighing them separately in air and ethyl iodide. The difference in the densities between the gauge and shoulder sections was attributed to the presence of excess cavities in the gauge section as a result of deformation.

3. Results

The microstructures of the tensile specimens annealed for 24–450 h were equiaxed. Two initial microstructures, upon annealing for 24 and 250 h, are given in Fig. 1. While the tensile specimens having the microstructure as shown in Fig. 1a (d = 7.6 μm) were used to study the influence of strain rate and test temperature on flow stress and microstructural evolution, the specimens with varying initial grain sizes were used to examine the effect of grain size.

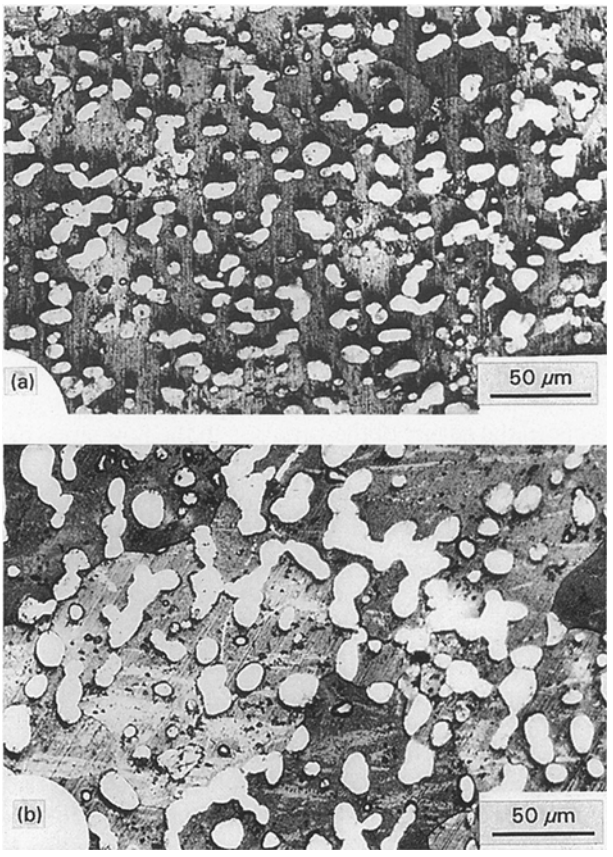

Figure 1 Initial microstructures obtained after annealing at 535 °C for (a) 24 h and (b) 250 h.

3.1. Flow behaviour

3.1.1. Effect of strain rate

Separate tensile specimens were deformed to failure at constant initial strain rates in the range from 5×10^{-6} to $2 \times 10^{-2}\ s^{-1}$ at a test temperature of 400 °C, and from 2×10^{-5} to $2 \times 10^{-2}\ s^{-1}$ at 540 °C. The stress–strain (σ–ε) curves are presented in Fig. 2. The σ–ε curves in many cases have not been drawn up to failure because the occurrence of necking, as judged from a steep drop in stress, causes an ambiguity in calculating the true stress.

It is seen that the flow stress at a fixed strain decreases with strain rate. The σ–ε curves generally show strain hardening in the beginning. With the decrease in strain rate the strain hardening diminishes, showing a complete disappearance, especially, at $\dot{\varepsilon} = 2 \times 10^{-5}$ and $1.1 \times 10^{-4}\ s^{-1}$ at 540 °C. The strain hardening is followed by a region of constant flow

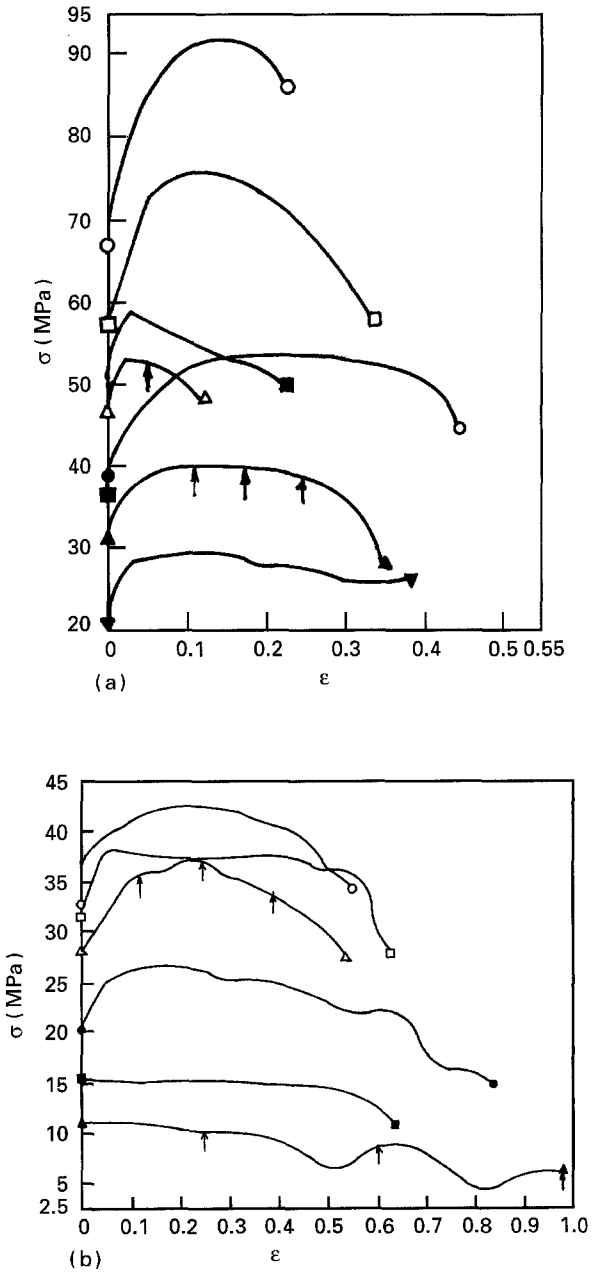

Figure 2 σ–ε curves at various strain rates at (a) 400 °C and (b) 540 °C, (d_0 = 7.6 μm). $\dot{\varepsilon}(s^{-1})$; (○) 2×10^{-2}, (□) 5×10^{-3}, (△) 1.1×10^{-3}, (●) 5×10^{-4}, (■) 1.1×10^{-4}, (▲) 2×10^{-5}, (▼) 5×10^{-6}.

stress, the extent of which increases with a decrease in strain rate and increase in temperature. Towards the end of the σ–ε curves, the flow stress is seen to decrease with increasing strain.

The σ–ε curves at various strain rates were used to obtain σ–ε̇ data at fixed strain levels as well as at the peak stresses. Then, log σ versus log ε̇ plots were made at various strains. The initial strain hardening, at most of the strain rates, Fig. 2, resulted in a shift in the log σ–log ε̇ curves towards higher flow stress. Subsequently, the log σ–log ε̇ curves were found to be independent of strain level. Only towards the final strains, did the log σ–log ε̇ curves move to lower flow stress. The log σ–log ε̇ plots based on the yield points and peak stresses at the two temperatures are given in Fig. 3.

The log σ–log ε̇ curves at 400 °C delineate two regions with a smaller slope, m, at the higher strain rates and a larger m at the lower strain rates. At 540 °C, however, there appear three regions with smaller m at the lower and higher strain rates; in the intermediate strain-rate range, m becomes maximum. The values of m, calculated from the slopes of log σ–log ε̇ plots at various strain levels, are given in Table I. Also given are the p and Q values which will be described later. At lower strain rates, m increases from 0.19 to 0.36 with increasing strain at 540 °C, whereas at 400 °C, m seems to be smaller at large strains. At higher strain rates, however, there is no systematic influence of strain on m but it is seen to be greater at 400 °C than that at 540 °C.

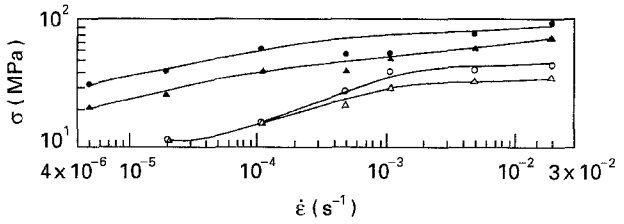

Figure 3 Log σ–log ε̇ curves at (▲, ●) 400 and (△, ○) 540 °C obtained from Fig. 2. The two curves correspond to (▲, △) the yield (ε = 0.002) and (●, ○) peak stresses.

3.1.2. Effect of temperature

At constant temperatures in the range 400–540 °C, the effect of temperature on flow stress was investigated at $\dot{\varepsilon} = 2 \times 10^{-5}$ and $1.1 \times 10^{-3}\ s^{-1}$. While the σ–ε curves at the minimum and maximum test temperatures have been already shown in Fig. 2, the σ–ε curves at the intermediate temperatures are presented in Fig. 4.

The σ–ε curves at both the strain rates show the decrease in flow stress with an increase in temperature. At the lower strain rate, Fig. 4a, the flow stress first increases with strain then it goes through ups and downs. At the higher strain rate, the initial strain hardening is followed by either strain softening at lower temperatures, or by the region of constant flow stress at higher temperatures, Fig. 4b.

Apparent activation energy for deformation was calculated from the flow-stress data as a function of temperature at fixed strain levels and strain rates according to the relation

$$Q = nR\left[\frac{\partial \ln \sigma}{\partial (1/T)}\right]_{\varepsilon,\, d,\, \dot{\varepsilon}} \qquad (2)$$

For this, the mean n values between 400 and 540 °C were taken from Table I at various strain levels. The Arrhenius plots for the yield and peak stresses at $\dot{\varepsilon} = 2 \times 10^{-5}$ and $1.1 \times 10^{-3}\ s^{-1}$ are shown in Fig. 5.

The values of Q from regression analysis at selected strain levels are included in Table I, which are noted to be greater at the higher strain rate with the mean being 224 and 386 kJ mol^{-1} at $\dot{\varepsilon} = 2 \times 10^{-5}$ and $1.1 \times 10^{-3}\ s^{-1}$, respectively. Although, at any strain, only one value of Q is given for the entire temperature range investigated, the Arrhenius plots suggest the possibility of two different values of Q based on the temperature range. This is illustrated by drawing two dashed lines instead of one solid line in Fig. 5. The activation energy in the higher temperature range, above a critical temperature, T_c, is estimated to be greater than that in the lower temperature range. For instance, the activation energy, using peak stresses, is found to be 482 kJ mol^{-1} above T_c as compared to 100 kJ mol^{-1} below T_c at $\dot{\varepsilon} = 1.1 \times 10^{-3}\ s^{-1}$.

TABLE I Values of m, Q and p at selected strain levels

		m				Q (kJ mol^{-1})		$p(T = 540\,°C)$	
	Strain level, ε	540 °C		400 °C		$\dot{\varepsilon} = 2 \times 10^{-5}\ s^{-1}$	$\dot{\varepsilon} = 1.1 \times 10^{-3}\ s^{-1}$	$\dot{\varepsilon} = 2 \times 10^{-5}\ s^{-1}$	$\dot{\varepsilon} = 1.1 \times 10^{-3}\ s^{-1}$
		II[a]	III	II[a]	III				
At peak stress, σ_p		0.33	0.04	0.2	0.17	271.7	503.6	−0.50	5.61
	0.002	0.19	0.06	0.19	0.13	199.6	388.8	0.83	4.27
	0.02	0.23	0.07	0.24	0.13	220.5	454.0	0.62	3.20
	0.05	0.28	0.02	0.22	0.16	216.0	461.9	0.15	9.66
	0.11	0.32	0.07	0.21	0.18	207.4	275.9	0.15	2.68
	0.16	0.32	0.06	0.18	0.16	229.7	233.7	0.11	1.98
	0.22	0.34	0.05	0.16	0.13	225.9	–	−0.03	0.91
	0.29	0.36	0.06	–	–	–	–	–	–
	0.3	0.36	0.08	–	–	–	–	–	–
Average		0.3	0.05	0.20	0.15	224.4	386.3	0.07	4.04

[a] Although the m values are smaller than that for the normal Region II, the slopes of log σ versus log ε̇ plots are distinctly greater than that at the higher strain rates.

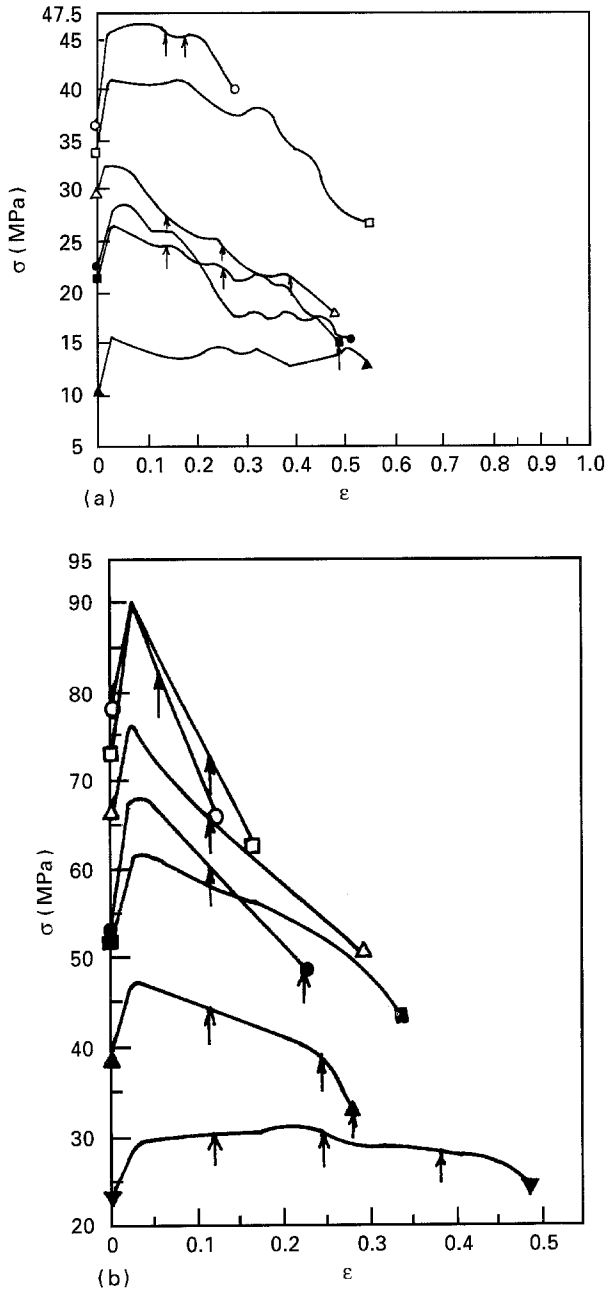

Figure 4 σ–ε curves at various temperatures and at strain rates of (a) $2 \times 10^{-5}\ s^{-1}$ and (b) $1.1 \times 10^{-3}\ s^{-1}$ ($d_0 = 7.6\ \mu m$). T (°C); (a) (○) 420, (□) 440, (△) 460, (●) 480, (■) 500, (▲) 520; (b) (○) 400, (□) 420, (△) 440, (●) 460, (■) 480, (▲) 500, (▼) 520.

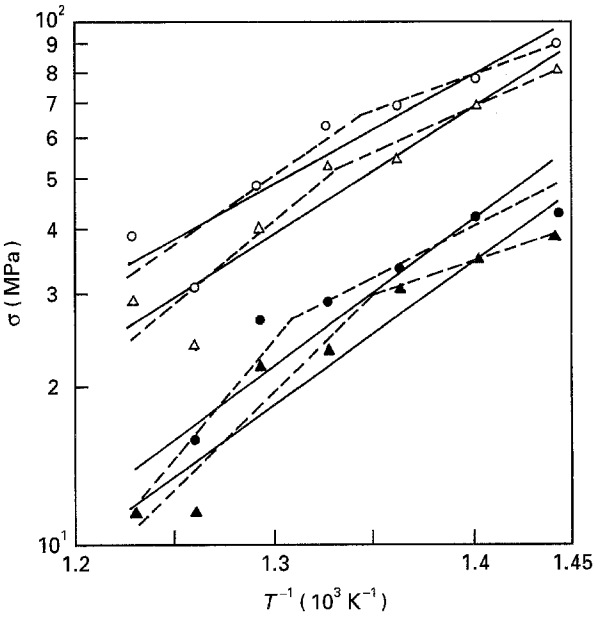

Figure 5 Arrhenius plots for determining the activation energy for deformation at (▲, ●) $\dot{\varepsilon} = 2 \times 10^{-5}\ s^{-1}$, (△, ○) $\dot{\varepsilon} = 1.1 \times 10^{-3}\ s^{-1}$. For $\sigma_{0.002}$, Q/n = (▲) 51.35 and (△) 45.82 kJ mol^{-1}. For σ_{peak}, Q/n = (●) 53.20 and (○) 39.66 kJ mol^{-1}.

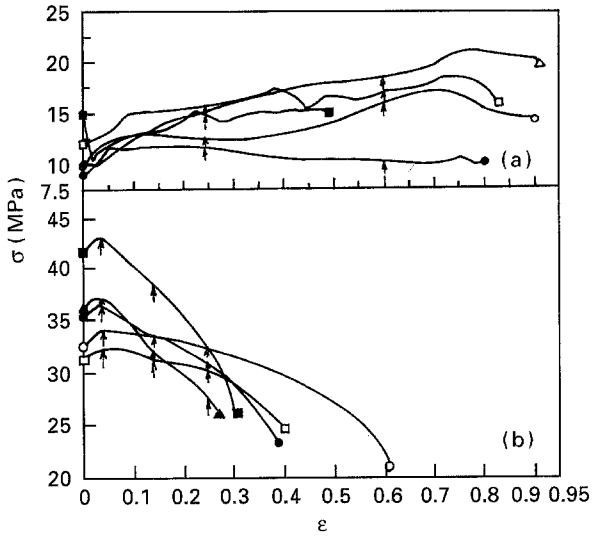

Figure 6 σ–ε curves from the specimens of various grain sizes at two strain rates, $\dot{\varepsilon}$: (a) $= 2 \times 10^{-5}\ s^{-1}$ and (b) $1.1 \times 10^{-3}\ s^{-1}$, ($T = 540$ °C) d(μm): (○) 7.6, (□) 10.1, (△) 13.1, (●) 15.9, (■) 20.6.

3.1.3. Effect of grain size

Tensile specimens having grain sizes of 7.6, 10.0, 13.1, 15.9 and 20.6 μm were deformed to failure at a constant temperature of 540 °C and at constant initial strain rates of 2×10^{-5} and $1.1 \times 10^{-3}\ s^{-1}$. The σ–ε curves at these two strain rates are given in Fig. 6a and b, respectively.

The σ–ε curves at $\dot{\varepsilon} = 2 \times 10^{-5}\ s^{-1}$, Fig. 6a, exhibit net strain hardening with intermittent strain softening. However, the σ–ε curve corresponding to $d = 15.9\ \mu m$ is noted to be an exception in which the flow stress starts falling from the beginning of deformation. Towards the end of deformation, the flow stress decreases in all the cases after attaining a distinct peak. The σ–ε curves at $\dot{\varepsilon} = 1.1 \times 10^{-3}\ s^{-1}$, Fig. 6b, show first the increase in stress up to $\varepsilon \leqslant 0.03$ then the decrease up to failure.

The σ–ε curves corresponding to the various grain sizes, but at the constant temperature and initial strain rates, were used to examine quantitatively the dependence of flow stress on grain size at fixed strain levels. The values of p, according to the equation

$$p = n \frac{\partial \ln \sigma}{\partial \ln d} \tag{3}$$

are given in Table I at selected strain levels. The values of n at the corresponding strains were taken from the m values at 540 °C which are listed in the table. The $\log \sigma$ versus $\log d$ plots for the yield stress, σ_y, at $\dot{\varepsilon} = 2 \times 10^{-5}$ and $1.1 \times 10^{-3}\ s^{-1}$, as well as for the peak stress, σ_p, at $\dot{\varepsilon} = 1.1 \times 10^{-3}\ s^{-1}$ are given in Fig. 7. The values of p are seen to be negligibly small at

most of the strain levels at $\dot{\varepsilon} = 2 \times 10^{-5}\ s^{-1}$. While, based on the yield stresses, p is found to be 0.83, its magnitude generally falls with an increase in strain. The values of p at $\dot{\varepsilon} = 1.1 \times 10^{-3}\ s^{-1}$ are noted to be larger than those at the lower strain rate.

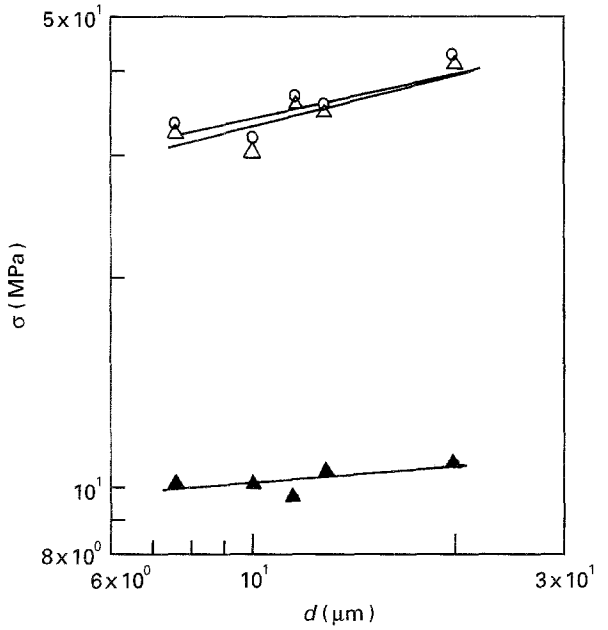

Figure 7 Log σ versus log d plots for determining p at (▲, □) yield and (○) peak stresses according to Equation 3. $\dot{\varepsilon} = 2 \times 10^{-5}$; (▲) $p/n = 0.16$. $\dot{\varepsilon} = 1.1 \times 10^{-3}$; $p/n =$ (□) 0.25, (○) 0.22, $T = 540\,°C$.

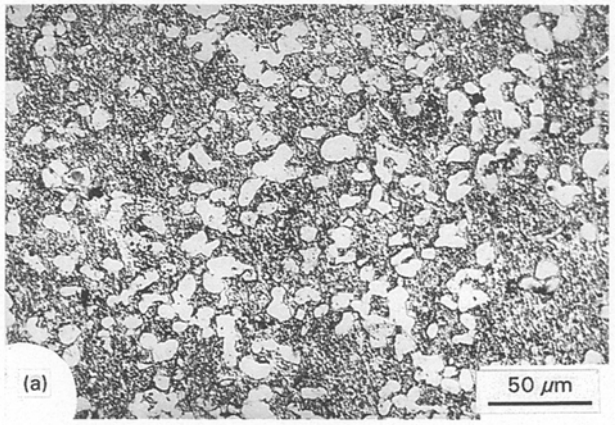

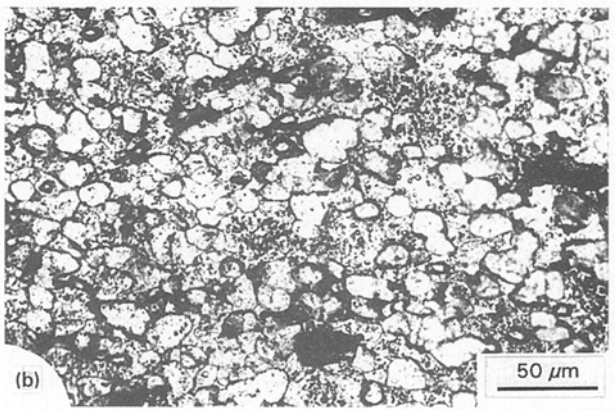

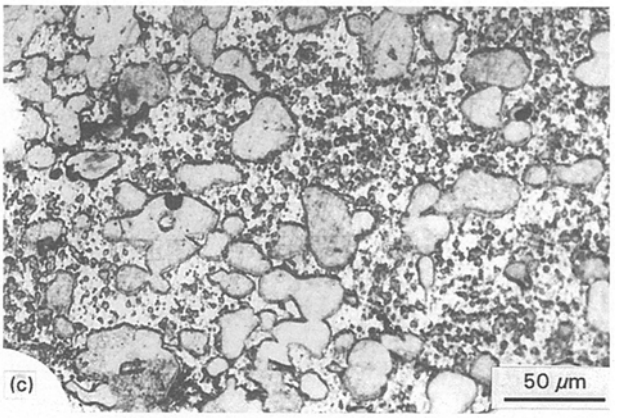

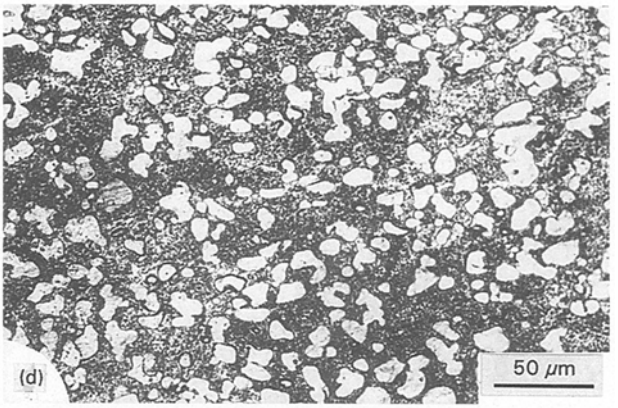

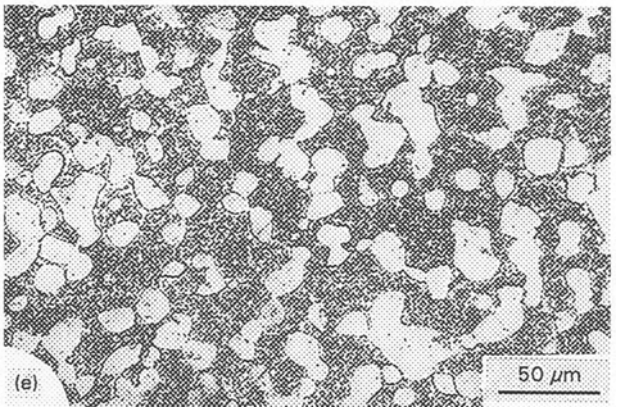

Figure 8 Influence of (a,b) strain, (a,c) strain rate, (a,d) temperature and (a,e) initial grain size on microstructure during deformation. Fig. 1a represents the initial microstructure for (a)–(d) whereas Fig. 1b represents that for (e). Test conditions ($\dot{\varepsilon}\ s^{-1}/T\,°C/\varepsilon/d_0\ \mu m$) are: (a) 2×10^{-5}/540/0.25/7.6; (b) 2×10^{-5}/540/1.66/7.6; (c) 1.1×10^{-3}/540/0.25/7.6; (d) 2×10^{-5}/460/0.25/7.6; and (e) 2×10^{-5}/540/0.25/15.9.

3.2. Microstructural evolution

The effect of deformation on grain size and cavity volume under different test conditions was followed as a function of strain.

The micrographs in Fig. 8 represent the microstructures resulting from the deformation at two strain rates (2×10^{-5} and $1.1 \times 10^{-3}\ s^{-1}$), two temperatures (460 and 540 °C), two strain levels (25% and 166%) and for two initial grain sizes (7.6 and 15.9 μm). When compared with the initial microstructures, Fig. 1, the grains are seen to remain equiaxed, but have undergone coarsening to varying extents. Fig. 9 shows some typical plots of d as a function of strain whereas the micrographs in Fig. 8 provide the qualitative

comparisons of grain-growth behaviour as a function of strain (a,b), strain rate (a,c), temperature (a,d) and initial grain size (a,e).

The d versus ε plots at $\dot{\varepsilon} = 2 \times 10^{-5}$ and $1.1 \times 10^{-3}\ s^{-1}$ and $T = 540\,°C$ suggest the grain growth to be slightly greater at lower strain rate but the reverse to be true at a lower temperature of 460 °C, especially, at $\varepsilon \geqslant 0.20$. When the initial grain size is larger ($d = 15.9\ \mu m$), the grain size upon deformation is seen to have reduced initially. At 540 °C, the reduced grain size remains constant up to $\varepsilon \approx 1.0$, beyond which it grows rapidly. At the higher strain rate of $1.1 \times 10^{-3}\ s^{-1}$ also, the reduction in the grain size is noticeable but the subsequent grain growth occurs from the early stage of deformation.

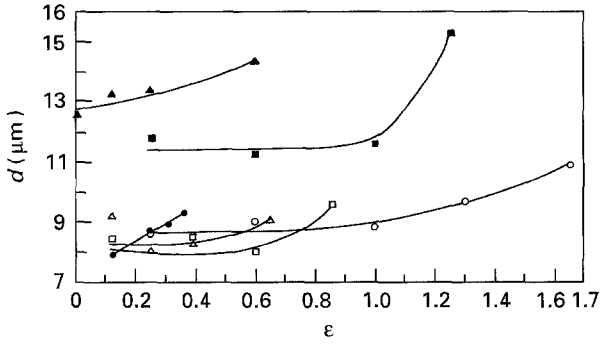

Figure 9 Variation in grain size as a function of strain illustrating the effects of temperature, strain rate and initial grain size. d_0 (μm); (○, □, △, ●) 7.6, (■, ▲) 15.9. T (°C); (○, □, ■, ▲) 540, (△, ●) 460. $\dot{\varepsilon}$ (s^{-1}); (○, △, ■) 2×10^{-5}, (□, ●, ▲) 1.1×10^{-3}.

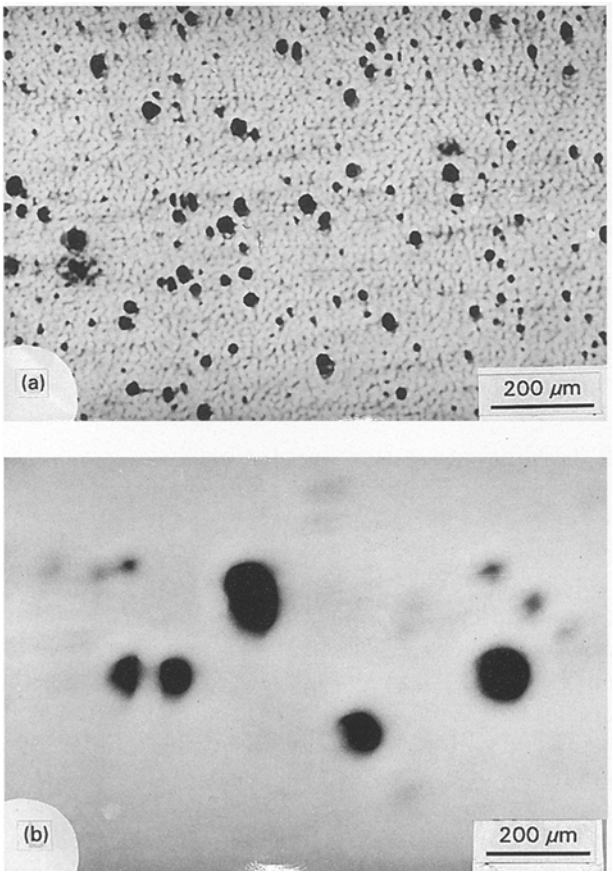

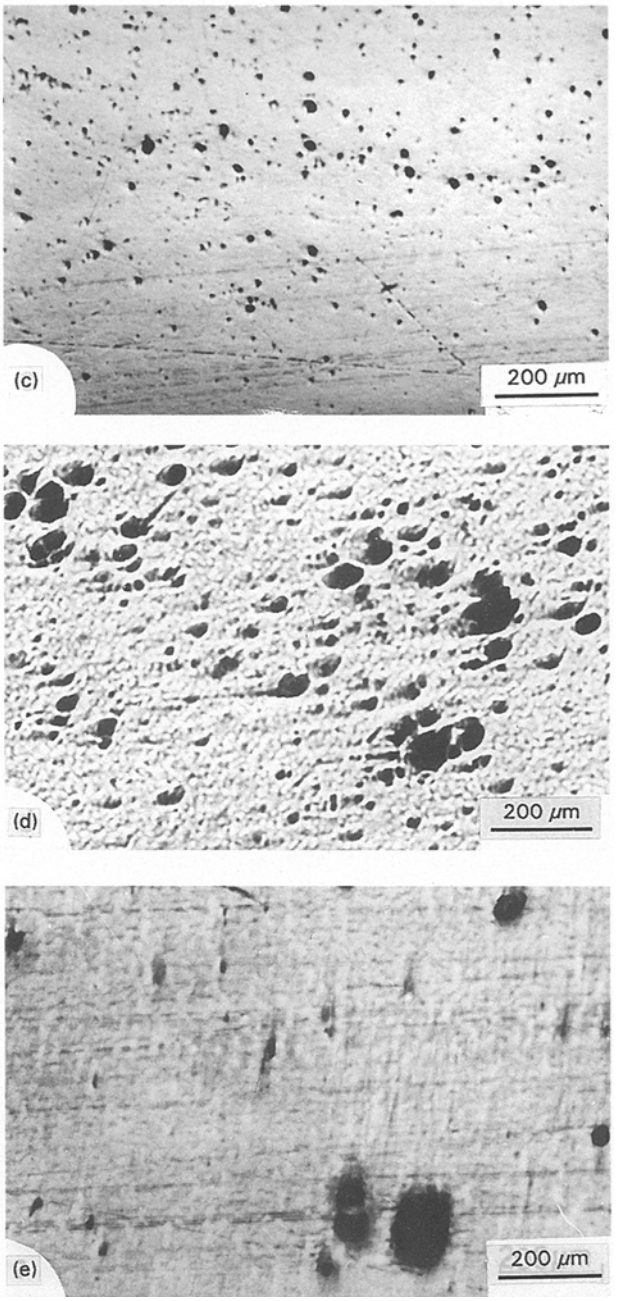

Figure 10 Influence of strain ((a) 0.25, (b) 1.30), strain rate ((a) $2 \times 10^{-5}\ s^{-1}$, (c) $1.1 \times 10^{-3}\ s^{-1}$), temperature ((a) 540 °C, (d) 460 °C) and initial grain size ((a) 7.6 μm, (e) 15.9 μm) on cavity volume ($\Delta V/V$, %). Test conditions ($\dot{\varepsilon}\ s^{-1}/T\ °C/\varepsilon/d_0\ \mu m$) are: (a) 2×10^{-5}/540/0.25/7.6; (b) 2×10^{-5}/540/1.30/7.6; (c) 1.1×10^{-3}/540/0.25/7.6; (d) 2×10^{-5}/460/0.25/7.6; and (e) 2×10^{-5}/540/0.25/15.9.

The micrographs in Fig. 10 exhibit cavities formed upon deformation at different conditions. These correspond to the same tensile specimens from which the micrographs in Fig. 8 were also taken. With the increase in strain (a, b), the cavity size is seen to increase and towards failure the number of cavities is noted to have reduced due to the dominance of cavity coalescence. With the increase in strain rate (a,c), the number of smaller sized cavities have increased. At the higher temperature of 540 °C (a), the number of cavities is seen to be more but their sizes are smaller as compared to those at the lower temperature of 460 °C (d). The larger grained materials depict larger cavities but fewer in number (e) in comparison to the smaller grained material (a).

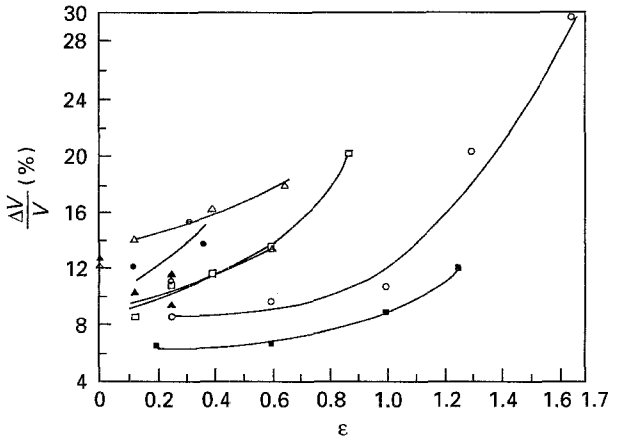

Figure 11 Variation in cavity volume as a function of strain illustrating the effects of temperature, strain rate and initial grain size. d_0 (μm): (○, □, △, ●) 7.6, (■, ▲) 15.9. T (°C): (○, □, ■, ▲) 540, (△, ●) 460. $\dot{\varepsilon}$ (s^{-1}): (○, △, ■) 2×10^{-5}, (□, ●, ▲) 1.1×10^{-3}.

The variation in cavity volume, ($\Delta V/V$, %), is plotted as a function of strain from the densitometry data in Fig. 11 at different test conditions in order to illustrate the influence of strain rate, test temperature and initial grain size. The cavity volume increases with strain in all the cases. At 540 °C, the cavity volume increases with strain rate but, at the lower temperature (460 °C) there appears an inverse relationship between the cavity volume and strain rate. At the lower strain rate of 2×10^{-5} s^{-1}, the cavity volume is seen to be higher at 460 °C than that at 540 °C, but the reverse is found to be the case at $\dot{\varepsilon} = 1.1 \times 10^{-3}$ s^{-1}. While the grain size shows some effect on cavitation, i.e. the larger the grain size the less is the cavity volume at $\dot{\varepsilon} = 2 \times 10^{-5}$ s^{-1}, the cavity volume at the higher strain rate appears to be insensitive to grain size.

In summary, the σ–ε curves show strain hardening, steady state and strain softening to varying extents, depending on strain rate, test temperature and initial grain size. Under such conditions, the parameters of the constitutive relationship vary significantly. The deviation from steady state flow is associated with concomitant grain growth and cavitation.

4. Discussion

4.1. Microstructural instability and σ–ε curves

Most of the σ–ε curves, Figs 2, 4 and 6, initially show strain hardening. The source for such strain hardening during superplastic deformation is believed [9] to be due to grain growth. If the p values at the yield points are considered to represent the true relation between stress and initial grain size, in view of no plastic deformation, then the grain sizes measured at various strains can be used to examine the contribution of grain growth to the observed strain hardening in the σ–ε curves. However, it should be noted that the continuous decrease in strain rate associated with the increasing strain should also lower the flow stress. Hence the instantaneous flow stress was corrected, σ_c, for the σ–ε curves at $\dot{\varepsilon} = 2 \times 10^{-5}$ and 1.1×10^{-3} s^{-1} and $T = 540$ °C by eliminating the effect of such changing strain rate. This was done by using the equation

$$\sigma_c = \sigma\left(\frac{L}{L_0}\right)^m \tag{4}$$

where σ is the flow stress from the original σ–ε curve, and L_0 and L are the initial and instantaneous gauge lengths. The resulting σ–ε curves, based on the m value at the yield points, are given in Fig. 12. As m also changes with strain, the σ–ε curves were also corrected by considering the varying m values given in Table I. The values of m at $\varepsilon > 0.39$ were, however, estimated from the σ–ε curves at $\dot{\varepsilon} = 2 \times 10^{-5}$ and 1.1×10^{-3} s^{-1}.

The grain-size data at various strain levels, d_f, under the above test conditions, were then used to calculate the flow stress expected, σ_f, according to the relation

$$\sigma_f = \sigma_y\left(\frac{d_f}{d_0}\right)^{p/n} \tag{5}$$

where σ_y is the yield stress of the specimen which had initially the grain size d_0. Again, in one case, the initial n ($= 1/m$) value and, in another case, the instantaneous n values were used; and the resulting σ–ε curves at $\dot{\varepsilon} = 2 \times 10^{-5}$ s^{-1} are shown in Fig. 12a. It can be noted that the σ–ε curve remains almost unchanged at small strains because the grain growth, Fig. 9, is insignificant. At large strains, however, the σ–ε curve based on the instantaneous grain size shows higher flow stress than actually observed. Thus, in spite of grain growth, the actual flow stress has decreased at the lower strain rate. On the other hand, at $\dot{\varepsilon} = 1.1 \times 10^{-3}$ s^{-1}, the flow stress increases with strain, Fig. 12b, although no significant grain growth has been observed. The strain hardening may then be the consequence of dislocation mechanisms.

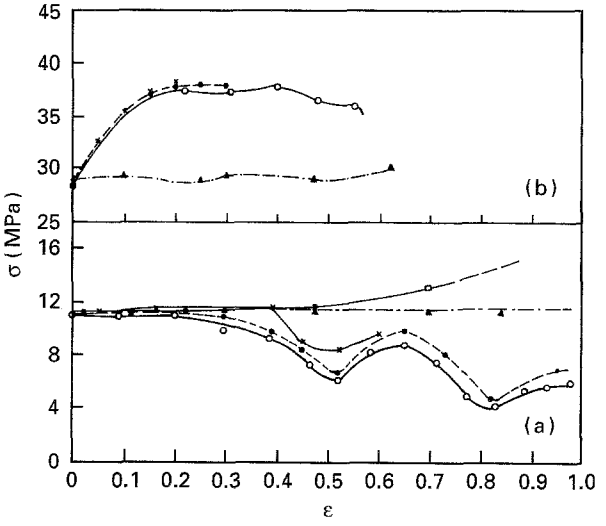

Figure 12 Corrections of σ–ε curves for constant true strain rates of (a) 2×10^{-5} s^{-1} and (b) 1.1×10^{-3} s^{-1} at 540 °C and $d = 7.6$ μm. Also included are the σ–ε curves corrected for the grain sizes measured at selected strain levels. (a) Constant speed; (●) constant true $\dot{\varepsilon}$ (m = (a) 0.19, (b) 0.06); (×) constant true $\dot{\varepsilon}$ (varying m); (▲) corrected for instantaneous d ((a) $m = 0.19$, p, 0.83), (b) $m = 0.06$, p, 4.27, (□) corrected for instantaneous d (varying m, $p = 0.83$).

In addition to grain growth, concurrent cavitation occurs. While in the early part of straining both are seen to be insignificant they increase with strain at large strains. The cavities are known [8] to lower the flow stress. Therefore, the difference between the σ–ε curves predicted on the basis of grain growth and that recorded from the tensile test, Fig. 12a, is suggested to be the result of cavity formation.

Strain softening, in the absence of cavitation, is caused by dynamic recrystallization [13]. While the σ–ε curves at $\dot{\varepsilon} = 1.1 \times 10^{-3}\,s^{-1}$, with a continuous drop in flow stress beyond the peak stresses, Figs 4b and 6b, are similar to those seen during continuous dynamic recrystallization, the zig-zag nature of the σ–ε curves resembles that during discontinuous dynamic recrystallization. However, the grain size data do not support the occurrence of dynamic recrystallization in the present study. If the effect of cavitation is thought to be similar to that of dynamic recrystallization, then the σ–ε curve with a continuously decreasing flow stress may be ascribed to continuous cavitation and the zig-zag σ–ε curves may correspond to discontinuous cavitation and intermittent grain-growth processes. The presence of peak stresses towards the end of deformation, following the prior strain softening, Fig. 6a, is reported in several cavitating superplastic materials, and it is explained [14] by the conventional strain-hardening effect in the ligaments between two cavities.

Knowing the opposite effects of grain growth and cavitation on flow stress, the variations in the grain size and cavity volume, presented in Figs 9 and 11, were used to relate qualitatively to the variation in stress of the corresponding σ–ε curves in Figs 2b, 4a, b and 6a, b. The following inferences could be drawn.

(i) The decrease in flow stress occurs due to cavitation in the absence of any significant grain growth.

(ii) When both the grain growth and cavitation occur rapidly, the flow stress increases first then decreases. In the case of a gradual increase in grain size and a slow or rapid increase in cavity volume, the σ–ε curves tend to be irregular.

(iii) The strain hardening in the beginning is related to grain growth in some cases only but not in all cases.

(iv) The σ–ε curve with steady state, showing no effect of strain on flow stress, is seen when both the grain growth and cavitation are negligible.

4.2. Non-steady state and constitutive relationship

The parameters of the constitutive relation for high-temperatue deformation, Equation 1, in some cases vary significantly with strain, whereas in other cases they are almost insensitive to strain, Table I. The variations in the parameters suggest them to be rather the apparent values because the stress should not change with strain and the grain size should also remain constant during steady-state deformation. The magnitude of the deviation from the true values of m, Q, and p representing steady state, depends on how much the work hardening or strain softening influence the values of σ (namely σ_2 and σ_1) in the numerator, at the two test conditions in the denominator of equations such as Equations 2 and 3. The effect of non-steady state flow on m, Q and p has been discussed elsewhere [15]. Some amount of prior straining of all the tensile specimens has been found [16] to be useful in order to minimize the influence of non-steady state flow on the parameters of the constitutive relation in the Pb–Sn eutectic alloy. The σ–ε curves and the concomitant microstructural evolution in the present study, however, do not suggest such prestraining, because, in most of the cases the flow stress increases and/or decreases with increasing strain up to failure.

In the absence of a true steady-state behaviour, the parameters at the yield point or that based on the peak stresses, if the latter occur at low strains, can be more meaningful. At higher temperature and lower strain rates, $m > 0.3$ (Table I), suggests that a superplastic property may prevail under these conditions. The activation energies for deformation under such conditions are comparable with the activation energy for deformation of θ phase [17] and the lattice diffusion in copper ($211\,kJ\,mol^{-1}$) [18].

The values of m and Q, which conform with those of natural power law [3], suggest the deformation to result from dislocation motion, as discussed by Čadek [3]. However, p is found to be 0.83 on the basis of yield stress data. This value is in agreement with the Gifkins' recovery creep model [19] ($p = 1$) which is based on accommodation of grain-boundary sliding by dislocation movement in triple-point folds.

The values of m at higher strain rates and relatively lower temperature ($n = 5$–8) support a dislocation climb creep mechanism, but the higher activation energy associated with this may be a consequence of threshold stress [3]. It is surprising, however, that the p value at the higher strain rate is greater than that in Region II and it is in variance with the behaviour ($p = 0$ or 1) that is known [2, 4] for Region III. Probably, the effect of cavitation dominates the flow behaviour, in which case p may not represent the true grain-size exponent.

5. Conclusions

Results of high-temperature deformation of the Al–24Cu alloy leads to the following conclusions.

1. Strain hardening occurs, especially in the early part of deformation, followed by discontinuous or continuous softening or hardening. Within the intermediate strains, at lower strain rates as well as at higher temperatures, however, the stress remains almost independent of strain.

2. Deformation results in accelerated grain coarsening and cavitation which, in turn, contribute to strain hardening and strain softening, respectively. However, the resulting grain sizes at lower temperatures and higher strain rates do not adequately account for the observed strain hardening.

3. Apparent m, p and Q values vary with strain. In spite of the variations, the magnitudes of m and Q at higher strain rates are in general agreement with the behaviour of superplastic materials in Region III; p, however, is much larger (average = 4). At lower strain

rates, $m = 0.19$, $Q = 272\ kJ\ mol^{-1}$ and $p = 0.83$, from the yield stress data, support the Gifkins' recovery creep model.

References

1. A. K. MUKHERJEE, J. E. BIRD and J. E. DORN, *Trans. ASM* **62** (1969) 155.
2. K. A. PADMANABHAN and G. J. DAVIES, "Superplasticity" (Springer-Verlag, Berlin, 1980).
3. J. ČADEK, "Creep in metallic materials" (Elsevier, Amsterdam, 1988).
4. A. K. MUKHERJEE, in "Plastic deformation and fracture of materials: materials science and technology – a comprehensive treatment", vol. 6, edited by H. Mughrabi (VCH Verlagsgeselischaft mbH Weinheim, Germany, and VCH, New York, 1993) p. 406.
5. T. G. LANGDON, *Metall. Trans.* **13A** (1982) 689.
6. J. PILLING and N. RIDLEY, "Superplasticity in crystalline solids" (Institute of Metals, London, 1989).
7. D. S. WILKINSON and C. H. CÁCERES, *J. Mater. Sci. Lett.* **3** (1984) 395.
8. B. P. KASHYAP and A. K. MUKERJEE, *Res. Mech.* **17** (1986) 355.
9. G. RAI and N. J. GRANT, *Metall. Trans.* **6A** (1975) 90.
10. B. P. KASHYAP and K. TANGRI, *Scripta Metall.* **20** (1986) 769.
11. P. K. BAKSHI and B. P. KASHYAP, *Scripta Metall. Mater.* **29** (1993) 1073.
12. P. K. BAKSHI and B. P. KAHSYAP, *J. Mater. Sci.* **29** (1994) 2063.
13. H. J. McQUEEN and J. J. JONAS, in "Treatise on material science and technology – plastic deformation of materials", Vol. 6, edited by R. J. Arsenault (Academic Press, New York, 1975) p. 393.
14. T. G. LANGDON and D. M. R. TAPLIN, *S. M. Arch.* **2** (1977) 329.
15. B. P. KASHYAP and A. K. MUKHERJEE, *Mater. Sci. Technol.* **1** (1985) 291.
16. B. P. KASHYAP and G. S. MURTY, *Mater. Sci. Eng.* **50** (1981) 13.
17. G. S. SOHAL, *Mater. Sci. Technol.* **4** (1988) 811.
18. S. J. ROTHMAN and N. L. PETERSON, *Phys. Status Solidi* **35** (1969) 305.
19. R. C. GIFKINS, *J. Aust. Inst. Met.* **17** (1973) 137.

Received 11 April 1994
and accepted 11 April 1995